Influence of Molecular Orientation and Melt Relaxation Processes on Glassy Stress−Strain Behavior in Polystyrene

Peter J. Hine,*,† Alan Duckett,† and Daniel J. Read‡

School of Physics and Astronomy, University of Leeds, Leeds LS2 9JT, UK, and Department of Applied Mathematics, University of Leeds, Leeds LS2 9JT, UK

Received October 26, 2006; Revised Manuscript Received January 16, 2007

ABSTRACT: This paper explores the relationship between the level of preferred molecular orientation at different length scales and the subsequent glassy stress/strain behavior of polystyrene. To produce samples with a range of orientation states, samples of a commercial polydisperse polystyrene (M_w = 274 000 g/mol, polydispersity = 2.74) were first drawn to a set draw ratio and then annealed for a range of times: subsequent to this the glassy stress−strain behavior of the various annealed samples was then measured. Appropriate annealing times, and temperatures, were informed by the molecular based theories for the melt state. In particular, annealing times were chosen to span the range between the entanglement time, τ_e, and the typical reptation time, τ_d. Differences in the deformation behavior were linked to measurements of the birefringence and thermal shrinkage, reflecting short-range orientation and orientation of the order of the entanglement length, respectively. Results showed that for short annealing times ($\sim\tau_e$) the birefringence fell almost immediately and that the true stress−strain curves measured for these samples could be superposed by shifting along the true strain axis by an amount which correlated with the sample birefringence. For longer annealing times, of the order of the Rouse time τ_R, the stress/strain curves were found to no longer superpose in the higher true strain region. The shape of the strain hardening curve was found to correlate very well with the measurement of thermal shrinkage of the samples obtained after annealing. Samples with different initial draw ratios (and hence different initial birefringence and shrinkage), but then annealed to have the same shrinkage, were found to show the same shaped strain hardening curve: that is, the higher strain region of the curves superposed.

1. Introduction

In recent years there has been significant progress in linking the dynamics of polymer molecules with their melt flow behavior.[1] This has built on the original work of de Gennes[2] and Doi and Edwards[3] with the recent work of, among others, Likhtman and McLeish.[4] Much of this theoretical progress has arisen from the insight that polymer chains of sufficient length in the melt state are *entangled* and that topological entanglements between polymer chains restrict their dynamics. Motion perpendicular to the contour length of the chain is suppressed by entanglements, giving rise to the common theoretical picture that each chain is confined within a "tube" by the surrounding chains. By building on this basic concept, it now appears to be possible, at least in the case of monodisperse linear polymers, to make an accurate theoretical prediction of measurements of linear and nonlinear rheology and then (by embedding the developed constitutive laws in fluid dynamics software) to predict behavior in nonuniform flow. This is exemplified by the recent study of Collis et al.,[5] who followed such a route with polybutadiene and polystyrene.

The goal of the present study has been to extend these ideas of linking molecular structure and mechanical properties to the solid state. Structure/property relationships in solid polymers is an extensively researched area, with both experimental and theoretical based studies, the majority of the studies looking at amorphous polymers. Some of the earliest experimental studies were carried out by Ward and co-workers working on poly(ethylene terephthalate) (PET).[6−9] It was clear that there are considerable differences in the birefringence/draw-ratio plots between PET drawn above and below T_g, which led Ward to suggest different mechanisms in these two temperature regions, affine above T_g and "pseudo-affine" below: for a review of these studies see ref 10 (and more recently Okumura,[11] also on PET). A key question is the relationship between the imposed macroscopic deformation and the strain at a molecular level. Neutron scattering studies on glassy polycarbonate and poly(methyl methacrylate) have confirmed that deformation is affine for long chains, and for length scales above the entanglement length, but have also shown, for shorter chains and for length scales of the order of a few monomer units, that the local deformation can diverge from the affine assumption.[12,13] Recently, an NMR study of segmental orientation in deformed cross-linked poly(methyl methacrylate)[14] demonstrated a strong difference between deformation above and below the glass transition temperature. The data were analyzed in terms of the apparent network density required to reproduce the observed levels of segmental orientation as a function of strain; it was found that the apparent network density for deformation in the glassy state was significantly higher than in the rubbery state. Previously, Kashiwagi, Folkes, and Ward in their NMR study of oriented PMMA[15] concluded that the deformation had been "pseudo-affine", implying enhanced orientation at the segmental scale. In their shrinkage studies of PET, Bhatt and Bell[16] suggested that, as temperatures approached T_g from above, the deformation continued to be rubberlike but with an increasing entanglement density. Furthermore, they suggested that with increasing deformation at the lower temperatures there was network slippage resulting in a birefringence/draw-ratio plot which was concave to the draw ratio, strongly reminiscent of the pseudo-affine model of Ward.[17] All of these studies suggest that there are deviations from affine behavior at short length scales especially around T_g and below, and these might mimic the "pseudo-affine" assumption.

† School of Physics and Astronomy.
‡ Department of Applied Mathematics.

10.1021/ma062474+ CCC: $37.00
Published on Web 03/14/2007

Recently, there has been some effort to model and understand the deformation of amorphous glassy polymers via molecular simulation, using techniques such as molecular mechanics,[18,19] molecular dynamics,[20,21] and dynamic Monte Carlo simulation.[22,23] Although the effective deformation rate in these simulations is much higher than in experiments (and is effectively infinite in the case of molecular mechanics, which does not include thermal motion), some interesting features emerge which potentially have experimental relevance. The molecular mechanics simulations[18,19] indicate that plastic relaxation events are highly cooperative and involve many (perhaps thousands of) atoms. This is also suggested by Capaldi et al.,[21] who obtain a transformation volume of 12 nm^3 based on an apparent activation volume of 0.21 nm^3 and a transformation strain of 0.017. Both Li et al.[22] and Chui and Boyce[23] examine the contribution of different types of interatomic force to the sample stress. At small strains, all types of interactions (bonded and nonbonded) make contributions to the increase in stress. However, both studies conclude that the observed strain hardening at large strains arises from *bonded* interactions (and is thus an intrachain effect). This latter observation is an important one: while it is conceptually plausible for strain hardening to arise both from intrachain interactions (orientation and stretching of individual chains) and from interchain interactions (e.g., via rearrangement of the locally packed structure), the simulations strongly suggest only the former is important.

The development of theoretical constitutive models to predict glassy stress−strain behavior has proceeded along classical lines with combinations of spring and dashpot elements (including 3D extensions of this concept). A common feature of the majority of such models is the use of a nonlinear viscous dashpot in series with a stiff spring to describe the small strain elastic response and yield of the material; in parallel with this, a weaker (sometimes nonlinear) spring provides strain hardening at high strains.[24−28] With respect to the strain hardening portion of the stress−strain curve, the simulations referred to above support the frequently proposed idea that the additional stress arises from orientation and stretching of polymer molecules (the strain hardening was shown to arise from bonded interactions). It appears common to describe this molecular orientation as occurring due to *entanglements* between polymer chains. The strain hardening stress in these constitutive models is thus formulated by appealing to rubber elasticity theory, using either a simple Gaussian rubber or nonlinear constitutive law.

Given that there is a common concept of "entanglements" in the description of both polymer melt flow behavior and strain hardening of amorphous glassy polymers, it is natural to ask whether these are, in fact, the same thing. The observations of the NMR study of Wendlandt et al.[14] demonstrate that they are not the same: the apparent network density for deformation in the glassy state is higher than in the rubbery/melt state. This is consistent with the observation that the strain hardening modulus in the glassy state is, typically, much larger than the melt plateau modulus.[29] Questions of this kind are important if one is interested in how melt processing affects subsequent solid-state deformation behavior after cooling: one needs an understanding of the development of molecular structure and orientation in both the melt and glassy states. It is known that flow in the melt state can produce different levels of molecular orientation at different length scales.[5,30,31] It is important to know which length scales are important in amorphous polymer deformation. One might, ultimately, hope to be able to predict the level of molecular orientation induced by a given flow and temperature history during processing and the effect this will have on solid-state deformation.

For the work reported here, the aim has been to establish how molecular orientation at different length scales affects the glassy stress−strain behavior of polystyrene. This has been achieved by looking at the effect of the combination of a controlled predeformation, followed by an annealing stage, on the true stress/true strain curve. Suitable annealing times and temperatures were chosen on the basis of molecular parameters described in Collis et al.[5] Birefringence and thermal shrinkage have been measured for the various orientation states, and these measurements have been correlated with the shape of the stress/strain curves. While the philosophy of the work of our group in this area, as exemplified by the published studies of Collis[5] and Wu,[32] has been to use monodisperse polymers, there is a drawback in that, in general, only ∼10 g of material is available. For the work reported here, the need to develop and establish a new set of experimental testing protocols meant that a more widely available polymer was advantageous. For that reason we have worked with a commercial polydisperse polystyrene.

2. Experimental Section

2.1. Sample Preparation and General Details. The material used throughout this study was a commercially available, polydisperse, polystyrene, BASF PS2, which had a weight-average molecular weight (M_w) of 274 000 g/mol and a polydispersity of 2.74. First, samples were produced for the orientation experiments. This was achieved using an in-house microspinner, set to 220 °C, which produced parallel strips of dimensions 13 mm wide and 0.25 mm thick. Birefringence measurements on these strips showed this to be zero, but thermal shrinkage measurements, carried out in a silicone oil bath at 125 °C for 1 h, showed a small amount of shrinkage. An additional annealing stage, of 1 h at 140 °C under a very light pressure, was found to reduce this shrinkage to zero, giving fully isotropic samples as the base for the subsequent tests.

In the next stage, samples were drawn to a set ratio at a fixed temperature, annealed at this temperature for a range of times, frozen, and then retested under uniaxial tension. These tests were carried out using an Instron Extra Series 5500 screw driven tensile test machine and a temperature-controlled cabinet. Following previous work at Leeds investigating molecular orientation in polystyrene,[33] we chose 115 °C as the temperature for the drawing and annealing tests. The choice of annealing times was informed from a knowledge of the various relaxation times involved with polystyrene, calculated from the fitting of linear rheology measurements to molecular based theories.[4] For a monodisperse polymer there are three important time scales, τ_e, τ_R, and τ_d, which are the entanglement, Rouse, and reptation times, respectively. τ_e is the time for a segment between entanglement points to relax and so is independent of molecular weight. For polystyrene this is given as 7.13×10^{-4} s at a temperature of 170 °C. From this the Rouse time at 170 °C (the relaxation of the whole chain in an unentangled state) can be calculated from $\tau_R = \tau_e Z^2$, where $Z = (M_w/M_e)$. The Rouse time is thought to be the time scale for retraction toward the equilibrium contour length of a polymer chain within its tube following a nonlinear deformation.[1] The reptation time, τ_d, is the characteristic time for curvilinear diffusion of the chain along the contour length of the tube and is given by the equation of Likhtman and McLeish[4] as

$$\tau_d = (3Z^3\tau_e)\left(1 - \frac{2C_1}{\sqrt{Z}} + \frac{C_2}{Z} + \frac{C_3}{Z^{3/2}}\right)$$

where $C_1 = 1.69$, $C_2 = 4.17$, and $C_3 = 1.55$. Time−temperature superposition is then used to determine the values of these three relaxation times at other temperatures.

As is seen from the above equations, the Rouse and reptation times are both dependent on molecular weight, so the equations

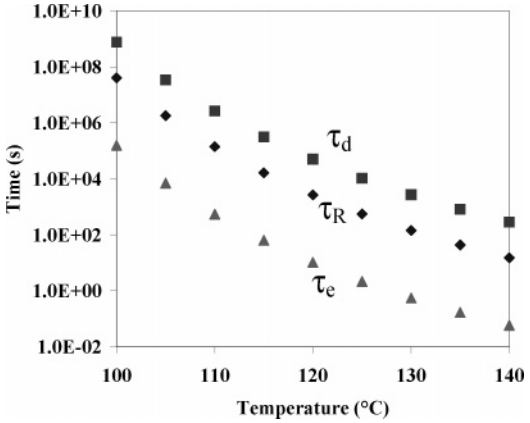

Figure 1. Calculated values for the three relaxation times, τ_e, τ_R, and τ_d, for BASF polystyrene PS2 (M_w = 274 000 g/mol).

are strictly applicable only to monodisperse polymers. The calculations for the BASF polydispersed polystyrene used in this work were therefore determined assuming that the appropriate molecular weight M_w is the weight-average value from GPC measurements (i.e., 274 000). As such, we use these calculations only to give a guideline as to time scales of the typical molecular processes occurring at the different annealing times. Obviously, there is a distribution of Rouse and reptation times in this material, brought about by the polydispersity. Figure 1 shows the results of these calculations for τ_e, τ_R, and τ_d against temperature, in the range of interest from 100 to 140 °C.

2.2. Tensile Testing. To find the appropriate temperature for the subsequent "glassy" stress−strain measurements on the annealed samples, uniaxial tensile tests were carried out at a range of temperatures. In the event, there was only a narrow temperature range (100−120 °C) where these tests could be carried out. If the temperature was too high, much greater than 120 °C, then significant molecular relaxation would occur during equilibrating the sample to the test temperature (about 600 s). Alternatively, at temperatures below 100 °C, the deformation was found to become localized, with the formation of a neck, and at even lower temperatures the samples broke in a brittle manner. A temperature of 105 °C was therefore considered optimum for the glassy retest experiments. As this is in the region of the glass transition temperature, accurate temperature control, to within ±0.1 °C throughout the oven, was required for repeatability.

While the initial drawing and annealing experiments, detailed in the previous section, were carried out at a constant displacement rate (100 mm/min, with an initial gauge length of 60 mm), the subsequent retest at 105 °C was undertaken at a constant true strain rate of 0.008 33 s^{-1}. The tests were carried out on an RDP servomechanical testing machine and an SPRI environmental chamber. An external voltage source from a computer was used to control the machine speed, and this was altered incrementally during the test to keep the true strain rate constant (based on the initial gauge length and the initial velocity and assuming homogeneous deformation). The sample strain was measured directly through the glass oven door using a Messphysik video extensometer, and postprocessing of these results confirmed that a constant true strain rate was indeed achieved in the tests.

2.3. Birefringence Measurements. The birefringence of the samples after the initial spinning, after drawing and annealing, and after subsequent retest was measured using a Carl Zeiss Jena microscope and an Ehringhaus compensator. As is normal with polystyrene, the direction of maximum change in birefringence was perpendicular to the main drawing direction due to the transverse orientation of the polar benzene ring group with respect to the main chain. For such a situation, relative changes in birefringence, as a result of tensile drawing and subsequent annealing, are designated as negative.

2.4. Thermal Shrinkage Measurements. Thermal shrinkage measurements were also carried out on the same range of samples

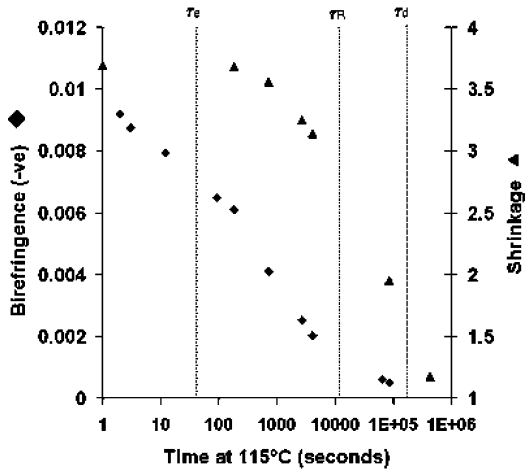

Figure 2. Birefringence (◆) and thermal shrinkage (■) of drawn and annealed samples vs annealing time at 115 °C after an initial draw at 115 °C of 4:1. The dotted lines show the positions of the three relaxation times at a temperature of 115 °C.

in a silicon oil bath. Following previous work at Leeds investigating molecular orientation in polystyrene,[33] a temperature of 125 °C and a time of 1 h were chosen to carry out these measurements. The samples to be measured were placed between mica sheets which were held together with paper clips at their edges, and their length before and after immersion in an oil bath was measured using a traveling microscope. The shrinkage, *S*, was then determined from

$$S = \frac{\text{original length}}{\text{final length}}$$

3. Results

3.1. Draw Ratio 4:1. For the first set of experiments, samples were drawn at a temperature of 115 °C to a draw ratio of 4:1 (at a speed of 100 mm/min with an initial gauge length of 60 mm, thus taking a time of 108 s) and then held at constant length for a range of times between 2 s and 5 days, at which point they were frozen using a freezer spray. The birefringence and thermal shrinkage were then measured on these samples before retesting at the lower temperature of 105 °C. For retesting, the samples were deformed at a constant strain rate of 0.00833 s^{-1}.

Figure 2 shows measurements of the birefringence and thermal shrinkage with annealing time at 115 °C for these samples: the positions of the three major relaxation times, τ_e, τ_R, and τ_d, calculated as described above, are also indicated in this figure. The results show that the birefringence begins to fall almost immediately with annealing at 115 °C but that the thermal shrinkage does not begin to fall until after a few minutes. This must be linked to the characteristic length scale involved in each relaxation process and how this relates to the macroscopic properties being measured.

Birefringence is a measure of the orientation of chain units at the monomer length scale, i.e., orientation at the smallest scales. While this local orientation does not decay completely until the sample becomes completely isotropic at the reptation time of the chains, Figure 2 indicates that the majority of the birefringence is relaxed by processes around the entanglement time scale, τ_e. This is an indication that the initial deformation was sufficiently rapid to induce orientation and stretching in short length scale modes of the chain, with characteristic lengths of order the entanglement size or less (note that the deformation time of 108 s is comparable to the entanglement time τ_e = 65 s at this temperature). These short length scale modes relax their contribution to the birefringence on time scales of

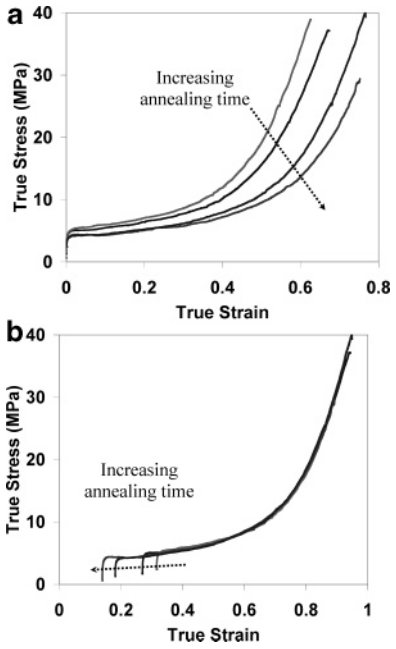

Figure 3. (a) True stress−true strain curves for 4:1 samples tested at 105 °C, after different annealing times at 115 °C between 0 and 90 s (constant true strain rate of 0.008 33 s^{-1}). (b) True stress−true strain curves for 4:1 samples tested at 105 °C, after different annealing times at 115 °C between 0 and 90 s (constant true strain rate of 0.008 33 s^{-1}). Data shifted along the true strain axis so that the strain hardening region superpose.

order the entanglement time, giving rise to the immediate drop in birefringence upon annealing evident in Figure 2.

The "shrinkage" indicates how far an unconstrained sample will shrink upon remelting. The shrinkage process is governed by a competition between stretched chain modes (which have a long relaxation time and which drive the shrinkage) and quickly relaxing modes (which act as a background viscosity to limit the shrinkage rate). Broadly speaking, the long-lived modes can be associated with melt entanglements, and the structure and orientation of the chains with respect to their entanglements govern the degree of shrinkage. Hence, the typical annealing time scales for loss of shrinkage are the Rouse time τ_R (chain retraction within the tube reduces the shrinkage necessary to balance the stress due to entanglements) and reptation time, as is evident in Figure 2.

Figure 3 shows the true stress−true strain curves of these samples when retested at a constant true strain rate: in this figure is shown results for annealing times between 0 and 90 s: First, in Figure 3a is shown the data as collected. As the annealing time is increased it is seen that the initial yield stress falls and that the onset of strain hardening moves to a higher true strain (the arrow indicates curves with increasing annealing time and decreasing birefringence). Second, Figure 3b shows these same curves but shifted along the true strain axis in order to superimpose the strain hardening regions: it is seen that the superposition is very good. Shifting of the stress−strain curves in this way was first proposed in another context by Brody[34] and has since been employed by Long and Ward[8] and Okumura,[11] among others.

Figure 4 shows data for an additional sample, annealed for 12 min; this is the earliest annealing time for which a drop in the sample shrinkage was observed. The stress−strain curve of this sample cannot be shifted so that it superposes in the entirety of the strain hardening region with the corresponding curves for the samples with shorter annealing time. It is possible, however, to shift so that the initial part of the strain hardening

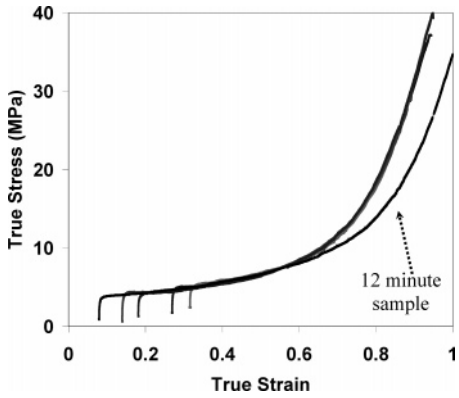

Figure 4. True stress−true strain curves for 4:1 samples tested at 105 °C, after different annealing times at 115 °C between 0 and 12 min (constant true strain rate of 0.008 33 s^{-1}). Data shifted along the true strain axis so that the region between strains of 0.4−0.6 superposes.

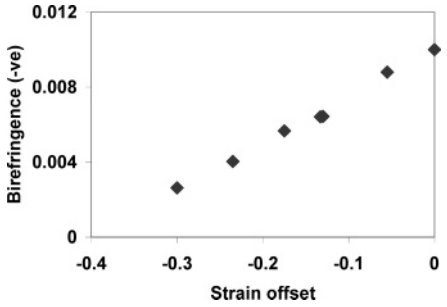

Figure 5. True strain offset required for superposition (in the true strain range 0.4−0.6) vs the birefringence after annealing at 115 °C.

region, up to a stress of roughly 7−8 MPa, superposes. We shall define the "weak strain hardening region" to be that part of the strain hardening curves for stresses less than 7 MPa, where the rate of increase of stress with strain is relatively shallow. It appears possible to obtain superposition of the weak strain hardening regions for different samples via a shift along the true strain axis. We define the "strong strain hardening region" to be that part of the strain hardening curves for stresses greater than 8 MPa, where the rate of increase of stress with strain is relatively strong and where superposition is not always possible. This definition of the strong and weak strain hardening regions is, necessarily, an operational one, yet it appears useful for the discussion of this and subsequent results. In particular, note that Figure 4 provides an indication that the shape of the strong strain hardening region may correlate with the sample shrinkage.

For samples annealed between times of 1 min and 24 h, Figure 5 shows the relationship between the strain offset (relative to the unannealed sample) required to get superposition of the stress−strain curves in the weak strain hardening region and the measured birefringence in the annealed samples before retesting. It is seen that this relationship is roughly linear. For all annealing times greater than 12 min, superposition was possible only in the weak strain hardening region.

3.2. Draw Ratio 3:1. Experiments were also carried out by drawing to 3:1 and annealing for the same range of times. Plots similar to Figure 2 were generated, and a similar relationship was found; that is, both the shrinkage and the birefringence fell with increasing annealing time (although starting from lower values) with characteristic times similar to those for the 4:1 drawn samples. Figure 6 shows a comparison of the effect of annealing on the birefringence (a) and thermal shrinkage (b)

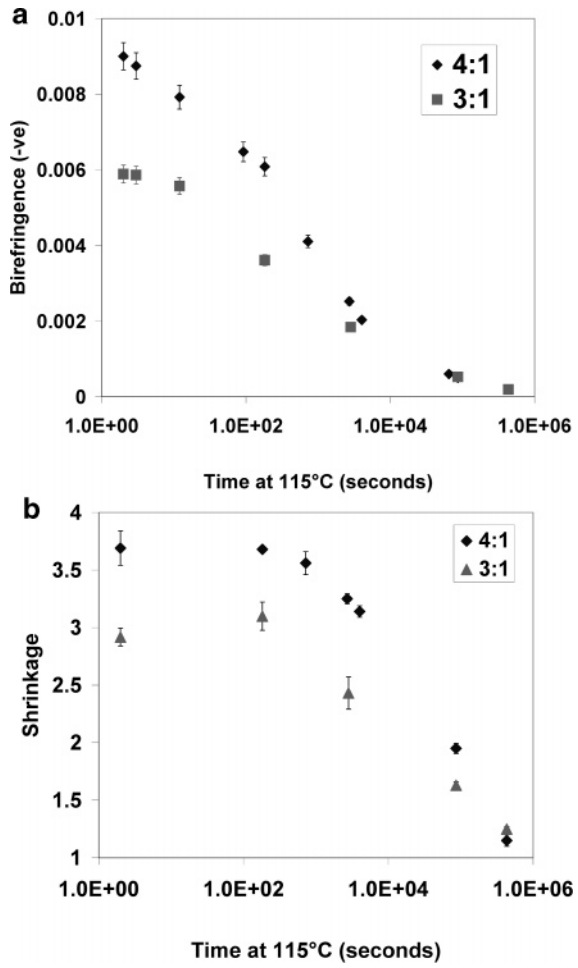

Figure 6. (a) Birefringence vs annealing time at 115 °C for an initial nominal draw ratio of 4:1 and 3:1. (b) Thermal shrinkage vs annealing time at 115 °C for an initial nominal draw ratio of 4:1 and 3:1.

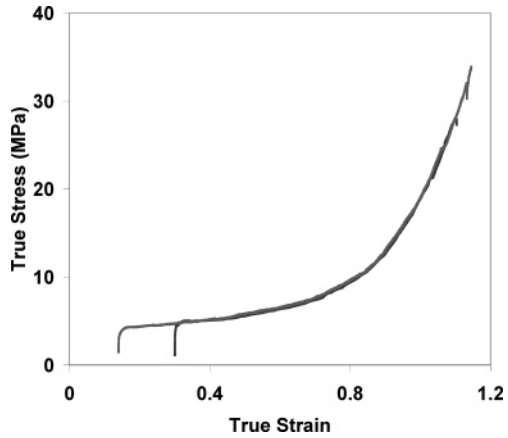

Figure 7. True stress−true strain curves for 3:1 samples tested at 105 °C, after annealing times at 115 °C for 0 and 90 s (constant true strain rate of 0.008 33 s^{-1}).

for samples initially drawn to a ratio of 3:1 and 4:1 and confirms a similar shape for both, albeit starting from lower values. Figure 7, which shows the true stress/true strain curves for a 3:1 drawn and frozen immediately sample and one annealed at 115 °C for 90 s, confirms that the true strain offset also works at this lower draw ratio. A similar superposition, in the weak strain hardening region, was found for a sample annealed for 47 min, albeit with a larger true strain offset.

In the previous section it was shown that there was a linear relationship between the true strain offset and the starting

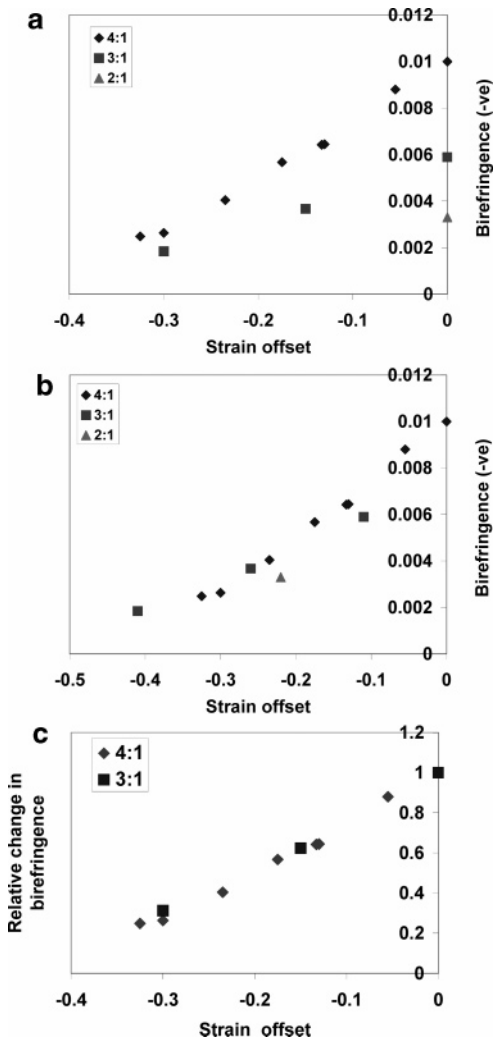

Figure 8. (a) Strain offset for superposition in the weak strain hardening region vs the starting birefringence of the various samples: results shown for draw ratios 4, 3, and 2. (b) Strain offset for superposition in the weak strain hardening region vs the starting birefringence of the various samples. The results are shifted with respect to the 4:1 frozen immediately sample. (c) Strain offset for superposition in the weak strain hardening region vs the starting birefringence of the various samples. The birefringence values were normalized with regard to the birefringence of the drawn and frozen sample for each draw ratio.

birefringence for the 4:1 drawn samples (Figure 5). In Figure 8a, the results for the 3:1 samples are plotted against these 4:1 results. It is seen that 3:1 results also show a linear relationship, but starting from a lower level of birefringence for the 3:1 frozen immediately after drawing sample (strain offset = 0), and also show a lower slope.

Figure 8b,c explores alternative methods for presenting the results of Figure 8a, for the different draw ratios. Results presented in the following section (Figure 9) will show that the samples drawn at different draw ratios and then frozen immediately can also be superposed in the weak strain hardening region. Using the 4:1 drawn and frozen sample as the reference, the results of the lower draw ratios shown in Figure 8a can be shifted by the true strain offset shown in Figure 9b and then replotted as shown in Figure 8b. It is seen that when presented in this way, the results fall on a rough master curve, suggesting a link between the absolute birefringence and the true strain offset. An alternative representation is to normalize the birefringence values for each draw ratio set, by the birefringence of the drawn and frozen immediately sample. The results

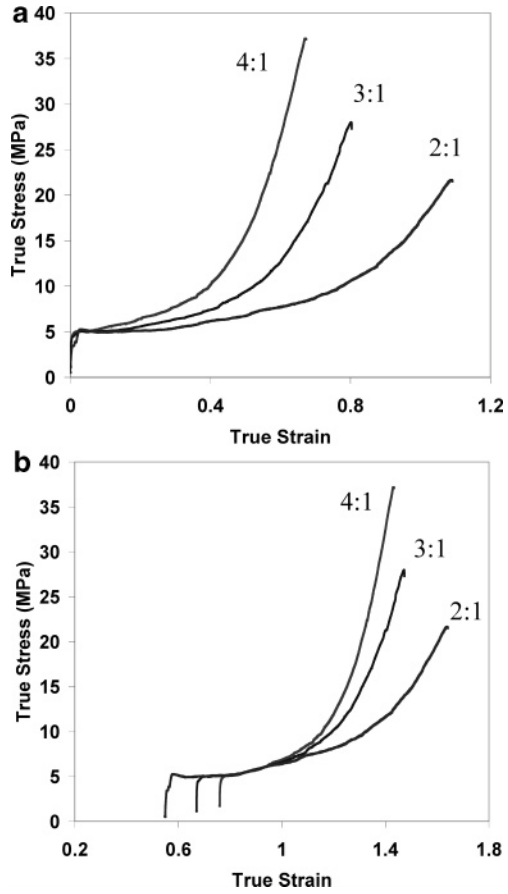

Figure 9. (a) True stress−true strain curves for samples drawn to 4:1, 3:1, and 2;1 at 115 °C, frozen immediately and then retested at 105 °C at a constant true strain rate of 0.008 33 s^{-1}. (b) True stress−true strain curves for samples drawn to 4:1, 3:1, and 2;1 at 115 °C, frozen immediately and then retested at 105 °C at a constant true strain rate of 0.008 33 s^{-1}. Shifted along the true strain axis to give superposition in the intermediate true strain region.

presented in this way (Figure 8c) suggest a strong link between the "relative" change in birefringence and the true strain offset. Further work is required to establish the most appropriate method for the presentation of these results.

3.3. Draw Ratios of 4:1, 3:1, and 2:1—No Annealing. Figure 9 shows a comparison of the true stress/true strain curves for samples drawn to three different draw ratios, frozen immediately, and then retested at 105 °C. Figure 9a shows the curves as measured and Figure 9b the curves after shifting to achieve a superposition in the weak strain hardening region. This was done so as to match the curves at a true stress of 7 MPa (at much higher stresses the curves begin to diverge significantly). These curves show a reasonable superposition in the weak strain hardening region but require a true strain shift for superposition due to a different starting birefringence (−0.0092, −0.0059, and −0.0033 for the 4:1, 3:1, and 2:1 samples, respectively). However, the strong strain hardening regions, at higher values of true strain, do not superpose. This remains consistent with the hypothesis that this latter portion of the curve is correlated with sample shrinkage. To clarify this point, the combined draw ratio at the true stress of 7 MPa has been calculated for the three samples and is shown in Table 1. So, for example, although the 2:1 sample requires a higher level of true strain to reach the true stress of 7 MPa, compared to the 4:1 sample, the combined draw ratio at this stress is lower than the 4:1 sample (3.2 compared to 4.8), leading to a lower strain hardening rate.

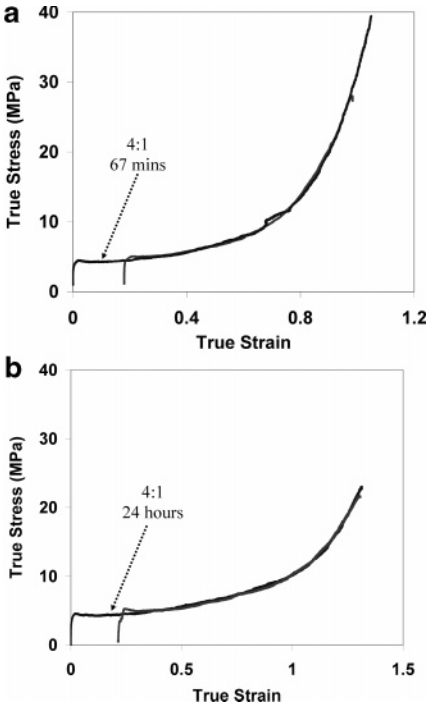

Figure 10. (a) A comparison of the true stress−true strain curves (tested at 105 °C at a constant true strain rate of 0.008 33 s^{-1}) for a sample drawn at 115 °C to 3:1 and frozen immediately and a sample drawn at 115 °C to 4:1 and annealed for 67 min. (b) A comparison of the true stress−true strain curves (tested at 105 °C at a constant true strain rate of 0.008 33 s^{-1}) for a sample drawn at 115 °C to 2:1 and frozen immediately and a sample drawn at 115 °C to 4:1 and annealed for 24 h.

Table 1. Product Draw Ratio (Initial Draw at 105 °C plus Retest at 115 °C) of Samples 1−3 in Figure 11 at a Stress Indicated by the White Circle

sample	initial nominal draw ratio (at 105 °C)	draw ratio for retest to 7 MPa (at 115 °C)	product nominal draw ratio
4:1	4	1.2	4.8
3:1	3	1.3	3.9
2:1	2	1.6	3.2

3.4. Further Annealing of 4:1 and 3:1 Samples. The results obtained so far suggest that we can, to first approximation, correlate the weak strain hardening region (and in particular the offset required to achieve superposition) with the sample birefringence and the strong strain hardening region with sample shrinkage. To investigate this supposition, additional annealing studies were carried out. In the first experiment, a 4:1 drawn sample was annealed for a time to give the same thermal shrinkage as a 3:1 drawn sample (67 min at 115 °C gave a shrinkage of 3.1 as shown from Figure 2). Figure 10a shows a comparison of the true stress−true strain subsequent retest of these two samples. It is seen that the weak and strong strain hardening regions both superpose very well (the samples have similar shrinkage) but that there is a true strain offset (due to a different level of birefringence: −0.0025 and −0.0059 for the 4:1 67 min and 3:1 frozen samples, respectively).

In the second, analogous, experiment, a 4:1 drawn sample was annealed for a time to give the same thermal shrinkage as a 2:1 drawn sample (24 h at 115 °C gave a shrinkage of 2.1 as shown from Figure 2). Figure 10b shows that again, in the entirety of the strain hardening region, the curves superpose very well but that there is a true strain offset due to a different birefringence (−0.0005 and −0.0033 for the 4:1 24 h and 2:1 frozen samples, respectively).

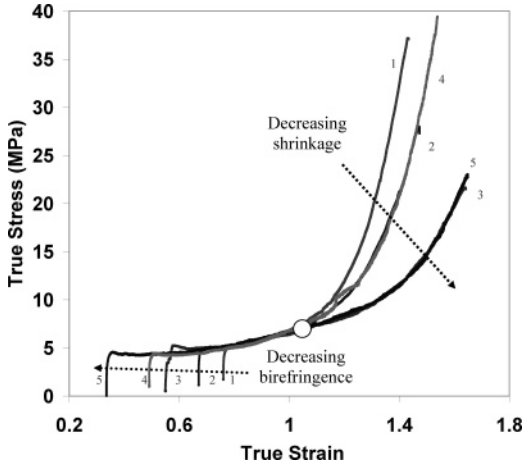

Figure 11. Comparison of all the results from Figures 9a and 10a,b.

Table 2. Birefringence and Thermal Shrinkage Values for the Samples 1−5 Shown in Figure11 (Measured before Testing)

sample	measured draw ratio	annealing at 115 °C	initial birefringence	initial thermal shrinkage
1	4.11 ± 0.10	no−frozen	−0.0092 ± 0.0005	3.69 ± 0.15
2	3.01 ± 0.04	no−frozen	−0.0059 ± 0.0006	2.91 ± 0.19
3	2.03 ± 0.03	no−frozen	−0.0033 ± 0.0002	1.90 ± 0.10
4	4.04 ± 0.08	67 min	−0.0025 ± 0.0001	3.14 ± 0.08
5	4.00 ± 0.07	24 h	−0.0005 ± 0.00003	1.95 ± 0.07

These two results support quite well the hypothesis that the strong strain hardening region is correlated with the sample shrinkage.

4. Discussion

The experiments described above can be summarized as follows. For all initial strains and annealing times, it was possible to superpose the weak strain hardening region of the stress−strain curves (<7 MPa) on retesting, via a shift along the true strain axis. The amount of shifting required correlates reasonably well (though not perfectly) with the sample birefringence. The strong strain hardening region appears to correlate with sample shrinkage measurements: samples with the same shrinkage would superpose in the entirety of the strain hardening region, once the appropriate shift for birefringence was made. To illustrate this, Figure 11 collects all the data from Figures 9a and 10a,b, and Table 2 details the initial draw ratio, annealing regime, and measured birefringence and thermal shrinkage for these five samples. Curves with the same thermal shrinkage were shifted such their strain hardening regions superposed (curves 2 and 4 and curves 3 and 5 as shown earlier in Figure 10, a and b, respectively), and all the curves were shifted to superpose at the intermediate true stress of 7 MPa as shown by the white circle in the figure.

As discussed in section 3.1, birefringence is a measure of the local segment orientation of the samples. Annealing for even short times (similar to or less than τ_e) was found to relax this birefringence rapidly, with an associated change in the shape of the stress/strain curve. With knowledge of just the sample birefringence, one is able to make a reasonable prediction of the yield stress of the samples, and the stress/strain curve up to the limit of the weak strain hardening region upon subsequent retesting. The fact that the birefringence, the yield stress, and the weak strain hardening region are affected by short annealing times, and that they are correlated, provides a strong indication that activated flow in the weak strain hardening region produces molecular deformations which are very much local in nature, involving correlations between a few statistical segment lengths at most. This finding is very much in agreement with that of Wendlant et al.,[14] who show that the apparent network density for deformations in the glassy regime (for PMMA) is equivalent to just 2−3 statistical segment lengths per affine chain strand and thus significantly higher than the entanglement density.

It is important, however, to discuss this result in the light of computer simulations,[18,19,21] which suggest that plastic relaxation events under flow are highly cooperative and involve many (thousands of) atoms. (As discussed in the Introduction, Capaldi et al.[21] obtain a transformation volume of 12 nm^3 based on an apparent activation volume of 0.21 nm^3 and a transformation strain of 0.017.) The question arises: if a plastic relaxation event involves a cooperative rearrangement of so many atoms over a (relatively) large volume, how is it that the flow is able to produce orientation in molecules at such short length scales? The apparent contradiction can be overcome provided one recognizes that a plastic relaxation event does not involve the molecules within the transformation volume exploring all their internal degrees of freedom; i.e., it does not equilibrate the whole transformation volume. Instead, it seems most likely that each plastic relaxation event constitutes a rearrangement of all the atoms involved, which displaces each such atom just a small distance away from the path it would take under a completely affine deformation. (We note that, in the simulations of Shenogin et al.,[20] a large distribution of local atomic strains were found near the yield point, but the very fact that the local strain could be defined at all suggests that individual atoms do not move far enough to separate completely from nearest neighbors.) For this reason, the size of the plastic transformation volume is not the important quantity for the chain dynamics; what matters is the rate at which the chains are able to explore their surrounding volume, and this is set by the frequency of plastic relaxation events and the effect that each such event has on a given chain. We may explore the simplest possible model, in which one considers that each plastic relaxation event involving a given monomer allows the monomer to make a "hop" of distance κb away from its affine path (where b is the monomer step size), and κ is a parameter we would expect to be less than, or of order, one. If we assume each such hop made by a monomer is uncorrelated with other hops, the number of hops required to equilibrate a monomer with its surroundings is of order $1/\kappa^2$ (the process is diffusive). But, a chain undergoing local hops can be described by the Rouse model for polymer dynamics,[3] for which the time required to equilibrate the internal degrees of freedom of a chain section of n monomers is a factor n^2 larger than the time taken to equilibrate a single monomer. Hence, the number of plastic relaxation events (per monomer) required to equilibrate a chain section of n monomers is n^2/κ^2. So, an important quantity is the number of plastic relaxation events, involving a given monomer, which take place within one unit of applied strain: this is just $1/\Delta\epsilon$ where $\Delta\epsilon$ is the transformation strain (taken to be 0.017 by Capaldi et al.[21]). Hence, equating n^2/κ^2 and $1/\Delta\epsilon$ gives the maximum number of monomers in a chain section which can equilibrate within one unit of applied strain, i.e.

$$n_c \approx \frac{\kappa}{\sqrt{\Delta\epsilon}}$$

Taking $\Delta\epsilon = 0.017$ and (very generously) $\kappa = 1$ gives $n_c = 8$. Sections of chain involving this number, or more, of monomers will be strongly deformed by the flow since they are not able to relax all their internal configurations. We may note that neither entanglements nor the size of the transformation volume

is important in this argument. A test of the validity of this argument could be made by computer simulation: one could straightforwardly examine the deviation of individual chains from their affinely deforming path using computer simulation and hence test the rate at which chains explore their surrounding volume.

With the use of the true strain shift, all the curves were found to superpose up to a stress of ∼7 MPa. If the stress optical law was to hold at the testing temperature that was used (105 °C), then in the region where they superposed, they should also have the same birefringence. This hypothesis was checked by a further experiment. A 4:1 sample drawn at 115 °C, and frozen immediately, was retested at 105 °C and taken to a true strain such that a true stress of 7 MPa was reached (in the plateau region of Figure 11 where all the curves superpose as shown by the white circle), at which point the sample was again frozen. A similar experiment was undertaken with a 2:1 sample, and then the birefringence of these two samples was measured. The results gave a value of -0.0235 ± 0.0005 for the 4:1 redrawn sample and -0.0228 ± 0.0014 for the 2:1 sample, showing that indeed, at the point given by the white circle (and presumably for all other points where the curves superpose), their birefringence was very similar.

The correlation between birefringence and strain offset given in Figure 8, however, is not perfect. We take this to be an indication that there is some dependence in the weak strain hardening region on aspects of the molecular orientation which are not measured by birefringence: either higher order moments of the segment orientation distribution function or variations in the contribution of different normal modes of the polymer toward the local segment orientation. Either of these could be affected by the precise temperature and strain history of the sample.

Nevertheless, it would appear that melt entanglements have little to do with the weak strain hardening region. However, the shape of the strong strain hardening region does correlate with sample shrinkage. To the extent that sample shrinkage can be related to the structure of the melt entanglements (and the annealing relaxation time for shrinkage does indicate this to be the case), we can conclude that behavior in the strong strain hardening region is related to melt entanglements and the orientation of chain sections on this larger length scale. Since the noncrossing constraints in the melt must be preserved in the glassy state, we speculate that the rate of increase of stress in this region is related to the distribution of topological entanglements and might involve chain sections between entanglements being pulled tight. Such a picture has previously been discussed in the context of crazing.[35]

We consider that two immediate extensions to this work might provide useful additional information. First, it is important to repeat these studies on monodisperse materials, in which the relaxation timescales are more clearly defined. Second, it would be informative to reduce the deformation temperature to values more significantly below the glass transition temperature. A possible criticism of this work is that the deformation temperature was too close to the glass transition temperature, and while we feel that lower temperatures would only serve to slow the chain dynamics further, it is important to test this experimentally. We note that there are suggestions in the literature for different modes of deformation close to, and well below, the glass transition temperature.[36]

5. Conclusions

Experimental results obtained in this paper, on polystyrene samples produced using a combination of an initial draw at 115 °C and a subsequent annealing step, have shown how the glassy stress−strain behavior at 105 °C is affected by molecular orientation at different length scales. The initial part of the stress−strain curve was found to correlate well with the measured birefringence, indicating a dependence on local orientation states. Annealing at times of the order of the entanglement time, τ_e, was seen to change the initial part of the curve, while leaving the shape of the later, strong strain hardening portion, unaffected. It was shown that the annealed curves could be shifted along the true strain axis such that the strain hardening regions superposed and that the amount of this true strain shift correlated with the sample birefringence. For longer annealing times, of the order of the Rouse time τ_R, the strong strain hardening regions were found to no longer superpose, with the gradient of this region falling with increased annealing. This reduction in gradient was found to correlate well with the measured thermal shrinkage, that is, orientation at a longer length scale, of the order of a few entanglements. Finally, samples with a different initial draw, but then annealed to have the same thermal shrinkage, were found to superpose in the entire strain hardening region, reinforcing the link between the state of orientation at the entanglement length scale with the strong strain hardening portion of the glassy stress−strain curve. Hence, prediction of the initial, weak strain hardening portion of the stress−strain curve can be made, to a first approximation, with only a knowledge of sample birefringence. Prediction of the entire curve requires knowledge of orientation at multiple length scales.

Acknowledgment. We thank the EPSRC for funding this study as part of the Microscale Polymer processing project. We also thank BASF for the supply of the polymer. Finally, we thank Paul Buckley and Davide De Focatiis (Dept. of Engineering Science, University of Oxford) and Leon Govaert (TUE, Eindhoven) for helpful discussions.

References and Notes

(1) McLeish, T. C. B. *Adv. Phys.* **2002**, *51*, 1379−1527.
(2) de Gennes, P. G. *J. Chem. Phys.* **1971**, *55*, 572−579.
(3) Doi, M.; Edwards, S. F. *The Theory of Polymer Dynamics*; Clarendon: Oxford, 1986.
(4) Likhtman, A. E.; McLeish, T. C. B. *Macromolecules* **2002**, *35*, 6332−6343.
(5) Collis, M. W.; Lele, A. K.; Mackley, M. R.; Graham, R. S.; Groves, D. J.; Likhtman, A. E.; Nicholson, T. M.; Harlen, O. G.; McLeish, T. C. B.; Hutchings, L. R.; Fernyhough, C. M.; Young, R. N. *J. Rheol.* **2005**, *49*, 501−522.
(6) Pinnock, P. R.; Ward, I. M. *Trans. Faraday Soc.* **1966**, *62*, 1308−1319.
(7) Gordon, D. H.; Duckett, R. A.; Ward, I. M. *Polymer* **1994**, *35*, 2554−2559.
(8) Long, S. D.; Ward, I. M. *J. Appl. Polym. Sci.* **1991**, *42*, 1911−1920.
(9) Long, S. D.; Ward, I. M. *J. Appl. Polym. Sci.* **1991**, *42*, 1921−1929.
(10) Ward, I. M.; Sweeney, J. *An introduction to the Mechanical Properties of Solid Polymers*, 2nd ed.; John Wiley and Sons Ltd.: Chicester, 2004.
(11) Okumura, W.; Ohkoshi, Y.; Gotoh, Y.; Nagura, M. *J. Polym. Sci., Part B: Polym. Phys.* **2003**, *41*, 2322−2331.
(12) Rossle, W.; Lindner, P.; Dettenmaier, M. *Physica B* **1989**, *156*, 414−416.
(13) Dettenmaier, M.; Maconnachie, A.; Higgins, J. S.; Kausch, H. H.; Nguyen, T. Q. *Macromolecules* **1986**, *19*, 773−778.
(14) Wendlandt, M.; Tervoort, T. A.; van Beek, J. D.; Suter, U. W. *J. Mech. Phys. Solids* **2006**, *54*, 589−610.
(15) Kashiwag, M.; Folkes, M. J.; Ward, I. M. *Polymer* **1971**, *12*, 697.
(16) Bhatt, G. M.; Bell, J. P. *J. Polym. Sci., Part B: Polym. Phys.* **1976**, *14*, 575−590.
(17) Ward, I. M. *Proc. Phys. Soc. London* **1962**, *80*, 1176−1188.
(18) Argon, A. S.; Bulatov, V. V.; Mott, P. H.; Suter, U. W. *J. Rheol.* **1995**, *39*, 377−399.
(19) Mott, P. H.; Argon, A. S.; Suter, U. W. *Philos. Mag. A* **1993**, *67*, 931−978.

(20) Shenogin, S.; Ozisik, R. *Polymer* **2005**, *46*, 4397−4404.
(21) Capaldi, F. M.; Boyce, M. C.; Rutledge, G. C. *Polymer* **2004**, *45*, 1391−1399.
(22) Li, J.; Mulder, T.; Vorselaars, B.; Lyulin, A. V.; Michels, M. A. J. *Macromolecules* **2006**, *39*, 7774−7782.
(23) Chui, C.; Boyce, M. C. *Macromolecules* **1999**, *32*, 3795−3808.
(24) Haward, R. N.; Thackray, G. *Proc. R. Soc. London, Ser. A* **1968**, *302*, 453.
(25) Boyce, M. C.; Parks, D. M.; Argon, A. S. *Mech. Mater.* **1988**, *7*, 15−33.
(26) Arruda, E. M.; Boyce, M. C. *Int. J. Plast.* **1993**, *9*, 697−720.
(27) Buckley, C. P.; Jones, D. C. *Polymer* **1995**, *36*, 3301−3312.
(28) Tervoort, T. A.; Smit, R. J. M.; Brekelmans, W. A. M.; Govaert, L. E. *Mech. Time-Depend. Mater.* **1997**, *1*, 269−291.
(29) van Melick, H. G. H.; Govaert, L. E.; Meijer, H. E. H. *Polymer* **2003**, *44*, 2493−2502.
(30) Bent, J.; Hutchings, L. R.; Richards, R. W.; Gough, T.; Spares, R.; Coates, P. D.; Grillo, I.; Harlen, O. G.; Read, D. J.; Graham, R. S.; Likhtman, A. E.; Groves, D. J.; Nicholson, T. M.; McLeish, T. C. B. *Science* **2003**, *301*, 1691−1695.
(31) Graham, R. S.; Bent, J.; Hutchings, L. R.; Richards, R. W.; Groves, D. J.; Embery, J.; Nicholson, T. M.; McLeish, T. C. B.; Likhtman, A. E.; Harlen, O. G.; Read, D. J.; Gough, T.; Spares, R.; Coates, P. D.; Grillo, I. *Macromolecules* **2006**, *39*, 2700−2709.
(32) Wu, J. J.; Buckley, C. P. *J. Polym. Sci., Part B: Polym. Phys.* **2004**, *42*, 2027−2040.
(33) De Francesco, A. University of Leeds, Leeds, 2002.
(34) Brody, H. *J. Macromol. Sci., Phys.* **1983**, *22*, 407−423.
(35) Han, H. Z. Y.; McLeish, T. C. B.; Duckett, R. A.; Ward, N. J.; Johnson, A. F.; Donald, A. M.; Butler, M. *Macromolecules* **1998**, *31*, 1348−1357.
(36) Argon, A. S.; Bessonov, M. I. *Philos. Mag.* **1977**, *35*, 917−933.

MA062474+